analytical chemistry

pubs.acs.org/ac

Article

A Rolling Circle-Amplified G-Quadruplex/Hemin DNAzyme for Chemiluminescence Immunoassay of the SARS-CoV-2 Protein

Rui Zhang, Jie Wu, Hang Ao, Jinling Fu, Bin Qiao, Qiang Wu,* and Huangxian Ju*

Cite This: *Anal. Chem.* 2021, 93, 9933−9938

Read Online

ACCESS | Metrics & More | Article Recommendations | Supporting Information

ABSTRACT: Sensitive detection of the SARS-CoV-2 protein remains a great research interest in clinical screening and diagnosis owing to the coronavirus epidemic. Here, an ultrasensitive chemiluminescence (CL) imaging strategy was developed through proximity hybridization to trigger the formation of a rolling circle-amplified G-quadruplex/hemin DNAzyme for the detection of the SARS-CoV-2 protein. The target protein was first recognized by a pair of DNA−antibody conjugates, Ab-1 and Ab-2, to form a proximity-ligated complex, Ab-1/SARS-CoV-2/Ab-2, which contained a DNA sequence complemental to block DNA and thus induced a strand displacement reaction to release the primer from a block/primer complex. The released primer then triggered a rolling circle amplification to form abundant DNAzyme units in the presence of hemin, which produced a strong chemiluminescent signal for the detection of the target protein by catalyzing the oxidation of luminol by hydrogen peroxide. The proposed assay showed a detectable concentration range over 5 orders of magnitude with the detection limit down to 6.46 fg/mL. The excellent selectivity, simple procedure, acceptable accuracy, and intrinsic high throughput of the imaging technique for analysis of serum samples demonstrated the potential applicability of the proposed detection method in clinical screening and diagnosis.

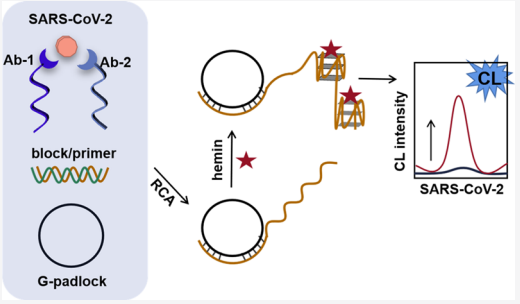

INTRODUCTION

Since the outbreak of the coronavirus epidemic in 2019, severe acute respiratory syndrome coronavirus type 2 (SARS-CoV-2) has spread at an unprecedented speed and scale.[1−3] The high fatality rate of SARS-CoV-2 and its susceptibility of infection result in an urgent need for sensitive and convenient detection methods for early and prompt screening and diagnosis of this disease to effectively control the dissemination of this infection. The general detection methods of SARS-CoV-2 include real-time polymerase chain reaction (RT-PCR) for the virus gene[4] and immunoassay for SARS-CoV-2-related proteins. The latter can be performed with enzyme-linked immunosorbent assay (ELISA),[5] gold immunochromatographic assay (GICA),[6] and chemiluminescence immunoassay (CLIA).[7] Although RT-PCR is a current standard method for SARS-CoV-2 diagnosis due to its high precision and specificity,[8,9] some data indicate that this detection technique is not suitable for all cases with clinical features of SARS-CoV-2, and serologic assay has become an indispensable tool as a complementary method for accurate diagnosis.[10] In serologic assay, commercially available ELISA is considered as a reliable detection method, but its efficiency is limited by laborious and time-consuming operation. Although a GICA-based method is convenient and time-saving for SARS-CoV-2 detection, its low detection sensitivity is not satisfactory for early and prompt screening of this disease.[11,12] Therefore, developing a convenient assay for the SARS-CoV-2 protein with high sensitivity is still an urgent need for epidemic diagnosis.

Benefiting from the advantage of the light emission produced by a specific chemical reaction, chemiluminescence (CL) can avoid the interference of autofluorescence from the biological specimen or stray excitation light, which normally exists in fluorescence-based assays for direct analysis of serum samples.[13] Thus, CL assay is considered as an ideal method for serologic assays[14−16] and has been used for immunological testing of SARS-CoV-2 infection.[17] Moreover, this technique possesses outstanding sensitivity, simple operation, and high throughput and can even be used for in vitro or in vivo imaging without a need for additional light sources.[18] More importantly, the CL technique can be conveniently combined with a flow injection technique for automated analysis[19] and some amplification strategies for further improving its sensitivity to meet the detection needs for low abundance proteins. For example, by using horseradish peroxidase or G-quadruplex DNA (G4)/hemin-functionalized gold nanoparticles as a labeling tag, two sensitive CL imaging immunoassay methods have been developed for detection of biomarkers.[20,21] The labeling tag can be conveniently amplified via a DNA-

Received: May 27, 2021
Accepted: June 28, 2021
Published: July 6, 2021

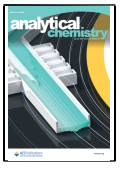

labeled antibody, which is used for both recognizing the target protein and extending the DNA scaffold via hybridization chain reaction (HCR) for loading of MnTMPyP[22] or forming signal switch via proximity hybridization for homogeneous CL bioanalysis.[23,24] Proximity hybridization has been used for formation of a G4/hemin DNAzyme to perform CL imaging of target proteins in serum samples.[25]

To achieve highly sensitive assay of the SARS-CoV-2 protein with high throughput, here, an amplified CL imaging strategy was developed by combining proximity hybridization with rolling circle amplification (RCA).[26] The amplified homogeneous CL imaging system was performed with a pair of DNA−antibody conjugates to recognize the SARS-CoV-2 protein, which formed a proximity-ligated complex, Ab-1/SARS-CoV-2/Ab-2, to induce a strand displacement reaction for releasing the primer from a designed block/primer complex. The released primer then triggered RCA with a C-rich circular DNA as a template to produce a duplicate sequence of G4,[27−29] which formed abundant DNAzyme units in the presence of hemin to produce a strong CL signal.[30−32] This strategy showed a specific response to the SARS-CoV-2 protein with a wide concentration range and a fg/mL-level detection limit. Owing to the advantages of CL imaging analysis, the proposed detection method possessed great promise for protein-related diagnosis.

EXPERIMENTAL SECTION

Reagents and Materials. Hydrogen peroxide (30%), 200 mM PBS (pH 7.2) buffer solution, and all DNA oligonucleotides were obtained from Sangon Biological Engineering Technology & Co., Ltd. (Shanghai, China). The DNA sequences are listed in Table S1. The recombinant SARS-CoV-2 nucleocapsid protein, SARS-CoV-2 vaccine, GICA test paper, and murine monoclonal SARS-CoV-2 antibodies 8B1 (Ab1) and 9B3 (Ab2) were provided by FANTIBODY (Chongqing, China). Hemin, luminol, maleimidobenzoic acid *N*-hydroxy succinimide ester (MBS), dimethyl sulfoxide (DMSO), and tris(2-carboxyethyl)phosphine hydrochloride (TCEP) were purchased from Sigma-Aldrich (St Louis, MO, USA). A silver-staining kit and a BCA protein kit were purchased from Biyuntian Biotechnology Co., Ltd. (Shanghai, China). An exonuclease III (Exo III), a DNA splint R ligase, a phi 29 DNA polymerase, and their corresponding buffers along with dNTP and BSA were bought from New England BioLabs (Beverly, MA, USA). An RCA reaction solution was freshly prepared by mixing the phi 29 DNA polymerase, dNTP, BSA, and its buffer in the ratios of 1:4:2:2 (v:v:v:v). All reagents were of analytical grade without further depuration. Ultrapure water from a Millipore water purification system was used for all experiments. The storing solutions of hemin (100 mM) and MBS (6.4 mM) were prepared by dispersing them into DMSO.

Apparatus. Polyacrylamide gel electrophoresis (PAGE) analysis was carried out with an electrophoresis analyzer (Bio-Rad, USA) and a Bio-Rad ChemiDoc XRS (Bio-Rad, USA). Ultraviolet−visible (UV−vis) absorption spectra were collected with a Varioskan Flash multimode reader (Thermo Scientific, USA). CL imaging was performed on a 96-well plate (Sangon Biological Engineering Technology & Co., Ltd., Shanghai, China), and the images were collected using a high-resolution cooled low-light CCD (BioImaging Systems ChemiHR 410 camera, UVP, USA).

Synthesis of DNA−Antibody Conjugates. According to previous studies,[33,34] DNA−antibody conjugates were prepared using MBS as a biofunctional connector. Antibody 1 (Ab1) (1 mg/mL) and antibody 2 (Ab2) (1 mg/mL) were first treated with excess 40-fold M MBS in 20 μL of 10 mM PBS (pH 7.2) for 2 h under low-frequency vibration, and excess MBS was removed by ultrafiltration (50 kDa Millipore, 10,000 rpm) to obtain Ab1-MBS and Ab2-MBS, respectively. Meanwhile, thiolated DNA 1 (24 μM) and DNA 2 (24 μM) were reduced with 150-fold M TCEP in 100 μL of 10 mM PBS (pH 5.5) for 2 h, and excess TCEP was removed by ultrafiltration (10 kDa Millipore, 12,000 rpm). Afterward, the reduced thiol-DNA 1 and thiol-DNA 2 were respectively mixed with Ab1-MBS and Ab2-MBS to incubate for 2 h, respectively. After unbound DNA 1 and DNA 2 were removed by ultrafiltration (100 kDa Millipore, 12,000 rpm), the concentrations of obtained DNA−antibody conjugates, DNA 1-Antibody 1 (Ab-1) and DNA 2-Antibody 2 (Ab-2), were quantized using a BCA protein kit. The above operations were performed at room temperature, and the purified Ab-1 and Ab-2 were stored in 50 μL of 10 mM PBS (pH 7.2) at −20 °C.

Preparation of Circular DNA. A G-padlock (10 μM) and a primer (10 μM) were first mixed in 25 μL of 10 mM PBS (pH 7.2) to anneal at 95 °C for 5 min, which was then slowly cooled to 25 °C and mixed with 2 μL of a splint R ligase (25 U/μL) and 3 μL of ligation buffer containing 500 mM Tris-HCl, 100 mM $MgCl_2$, 10 mM ATP, and 100 mM DTT to incubate for 5 h at 25 °C with gentle vibration. After three times ultrafiltration, 3 μL of Exo III (100 U/μL) and 6 μL of exonucleolytic buffer (CutSmart) were added in the product to adjust its volume with 10 mM PBS (pH 7.2) to 60 μL, which was then incubated at 37 °C for 5 h to obtain circular DNA and 65 °C for 20 min to terminate the reaction. The obtained circular DNA was stored at 4 °C for further use.

PAGE and Silver-Staining Analysis. A polyacrylamide gel (12%) was prepared with tris-borate-EDTA. The loading samples were prepared by mixing 5 μL of DNA or proteins and 1 μL of 5× loading buffer for 5 min incubation. After electrophoresis analysis for 60 min at 110 V, DNA lands were stained by placing the gel into a mixture containing nucleic acid fluorescent dye for 20 min and visualized with a molecular imager Gel XR, while the staining of protein lands was carried out with a silver-staining kit after being immobilized for 1 h with a mixture of 50% ethanol and 10% acetic acid and visualized with a common camera.

Thermal-Differential Absorption Spectroscopic (TDS) Detection. The G4 structure was verified with TDS measurement by recording the UV-absorption spectra under the conditions of unfolding and folding at temperatures above or below the melting temperature (T_m).[35] After measuring the absorption spectra of nucleic acids at different temperatures, the absorbance difference between 4 and 95 °C was calculated and used for forming a vertical difference map.

CL Response to the Primer. After 0.5 μL solutions containing different concentrations of the primer were mixed with 0.5 μL of circular DNA, 1.75 μL of PBS (10 mM, pH 7.2), and 2.25 μL of the RCA reaction solution to incubate for 2 h at 37 °C, 25 μL of PBS (10 mM) and 10 μL of hemin (5 μM) were added in the mixtures to incubate in the dark at room temperature for 20 min. A freshly prepared CL substrate mixture (20 μL) (10 μL of 20 mM luminol and 10 μL of 10 mM H_2O_2) was then added to collect the CL images with an exposure time of 30 s.

CL Imaging Detection of the SARS-CoV-2 Protein. Solutions (0.75 μL) containing different concentrations of the

https://doi.org/10.1021/acs.analchem.1c02229
Anal. Chem. 2021, 93, 9933−9938

SARS-CoV-2 protein or the serum samples were first added in 4.25 μL of the reaction mixture containing 0.5 μL of Ab-1 (10 ng/mL), 0.5 μL of Ab-2 (10 ng/mL), 0.5 μL of circular DNA, 0.5 μL of the block/primer complex (10 nM), and 2.25 μL of the RCA reaction solution to incubate for 2 h at 37 °C. Then, 25 μL of PBS (10 mM) and 10 μL of hemin (5 μM) were added in the mixture to incubate in the dark at room temperature for 20 min. Afterward, 20 μL of a freshly prepared CL substrate mixture (10 μL of 20 mM luminol and 10 μL of 10 mM H_2O_2) was added to collect the CL images using a CCD with an exposure time of 30 s. Spots were automatically identified using VisionWorksLS image acquisition and analysis software (UVP, USA). The CL intensity of each spot was calculated as the mean pixel intensity within a circle of a given radius.

RESULTS AND DISCUSSION

Antigen-Induced Formation of the G4/Hemin DNAzyme. In this work, a circular DNA, a pair of DNA−antibody conjugates (Ab-1 and Ab-2), a blocked primer (block/primer complex), and a phi 29 polymerase were mixed with the sample to perform target protein recognition and signal amplification (Scheme 1A). The circular DNA was prepared

Scheme 1. Schematic Diagrams of (A) CL Imaging for Detection of the SARS-CoV-2 Protein and (B) Preparation of Circular DNA

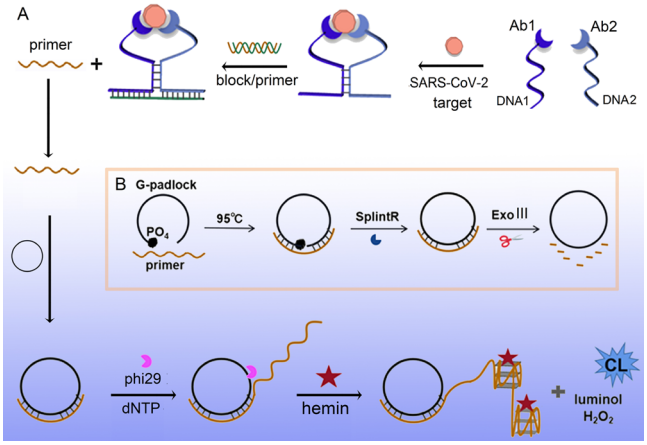

in advance via ligating of a G4-padlock with a primer and removing the hybridized primer through the cleavage behavior of Exo III (Scheme 1B). In the presence of the SARS-CoV-2 protein, the antibodies Ab1 and Ab2 in Ab-1 and Ab-2 recognized the protein to draw the DNA strands closer, which induced the generation of a proximity-ligated complex (named as Ab-1/SARS-CoV-2/Ab-2). Thus, the primer could be released from the block/primer complex via a strand displacement reaction, which triggered the RCA to produce a large amount of G4 duplicate sequences, leading to the formation of abundant DNAzyme units in the presence of hemin. Owing to the excellent catalytic ability of the DNAzyme to the oxidation of luminol by hydrogen peroxide, the amplified CL signal could be generated for sensitive detection of the SARS-CoV-2 protein in serum samples.

Characterization of Circular DNA. The formation of circular DNA was verified by CL imaging and TDS measurements. As shown in Figure 1A with the CL intensity range from 0 to 65,000, after the mixture of 0.75 μL of 100 pM

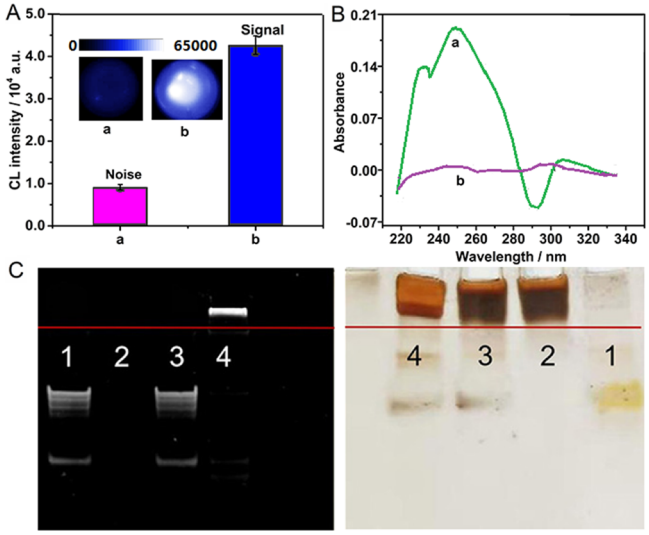

Figure 1. (A) CL intensity and (B) thermal difference spectra (TDS) for the mixture of 0.75 μL of 100 pM primer, 2.25 μL of the RCA reaction solution, and 1.75 μL of 10 mM PBS in absence (a) or presence (b) of 0.5 μL of circular DNA. (C) PAGE (left) and protein silver staining (right) of DNA 1 (1), Ab1 (2), DNA 1 + Ab1 (3), and Ab-1 (4).

primer, 2.25 μL of the RCA reaction solution, and 1.75 μL of 10 mM PBS was incubated and then mixed with hemin in PBS (10 mM) solution to perform CL imaging, a very weak CL signal could be observed, However, the presence of the obtained circular DNA led to a strong CL signal, indicating the successful triggering of RCA by the primer to produce G4 sequences. Compared to the flat TDS curve of the reaction mixture in the absence of circular DNA, which implied that no G4 existed in the mixture, the presence of circular DNA showed a sharp peak around 260 nm and a negative peak at 295 nm for the G4 structure (Figure 1B), further demonstrating the necessity of circular DNA for the formation of G4 sequences.

Characterization of DNA−Antibody Conjugates. As shown in Figure 1C, the strip of DNA 1 occurred at the same position in the lands loading DNA 1 and the mixture of DNA 1 and Ab1, indicating the absence of binding between DNA 1 and Ab1. Ab1 did not show its strip by staining with a nucleic acid dye. After DNA 1 was covalently bound with Ab1 using MBS as a biofunctional connector, the strip of Ab-1 showed much slower migration than DNA 1. The migration rate was similar to those observed for Ab1 and the mixture of DNA 1 and Ab1, indicating the successful preparation of DNA−antibody conjugates.

Feasibility of CL Imaging Assay for SARS-CoV-2. Both the RCA reaction solution and its mixture with circular DNA showed a very weak CL signal after they were incubated with hemin to perform the CL imaging (Figure 2a,b). The weak signal could be attributed to the slow oxidation of luminol by H_2O_2. After the primer was introduced into the mixture of the RCA reaction solution with circular DNA, a strong CL signal could be obtained (Figure 2c), indicating the formation of a G4/hemin DNAzyme to catalyze the oxidation reaction. However, the introduction of the block/primer complex into the mixture of the RCA reaction solution with circular DNA did not produce an obvious CL signal (Figure 2d), indicating the blocking of the primer by the block DNA. Moreover, the

https://doi.org/10.1021/acs.analchem.1c02229
Anal. Chem. 2021, 93, 9933−9938

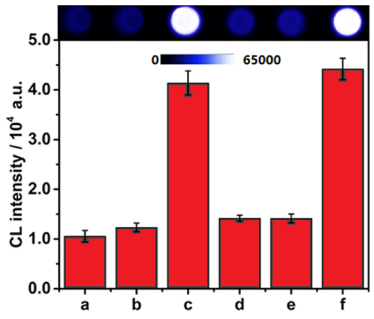

Figure 2. CL signals of (a) RCA reaction solution, (b) a + 0.5 μL of circular DNA, (c) b + 0.5 μL of 100 pM primer, (d) b + 0.5 μL of 10 nM block/primer, (e) d + 0.5 μL of 10 ng/mL Ab-1 + 0.5 μL of 10 ng/mL Ab-2, and (f) e + 0.75 μL of 20 pg/mL SARS-CoV-2 protein.

introduction of Ab-1 and Ab-2 without the presence of the target protein did not change the signal intensity (Figure 2e). The weak CL signal could be considered as the background or noise. After the SARS-CoV-2 protein was added in the mixture of Ab-1, Ab-2, the block/primer, circular DNA, and the RCA reaction solution to incubate for 2 h at 37 °C and then mixed with hemin to incubate in the dark for 20 min, the strong CL signal could be observed (Figure 2f), the same as the primer introduction in the mixture of the RCA reaction solution with the circular DNA primer, leading to an amplified CL method for detection of the SARS-CoV-2 protein.

Optimization of Detection Conditions. The concentration of hemin was a vital factor affecting the detection performance. Little hemin led to a low CL signal difficult to detect for observation, while too much hemin caused a high background. As shown in Figure 3A, the CL signal increased with the increasing concentration of hemin, which also resulted in increasing background. The maximum signal-to-noise ratio occurred for the hemin concentrations of 2 to 5 μM. Thus, 5 μM hemin was used as the optimal condition to obtain high sensitivity. In addition, the RCA time determined the length of the product chain and thus influenced the catalytic efficiency and CL intensity. The CL intensity increased with the increasing incubation time, and the signal-to-noise ratio tended to a maximum value after incubation for 2.0 h (Figure 3B), which was selected to perform simultaneous proximity hybridization, strand displacement reaction, and RCA.

CL Response to the Primer. Under the optimal conditions, the performance of CL imaging assay was first evaluated with primer-triggered RCA. As expected, the CL intensity increased with the increasing concentration of the primer, and the plot of the CL signal versus the logarithm of primer concentration showed good linearity in the range concentrations from 0.01 to 500 pM with the correlation coefficient of 0.9983 (Figure 4). This result guaranteed the feasibility of quantitative analysis for the target protein through proximity hybridization and primer-triggered RCA.

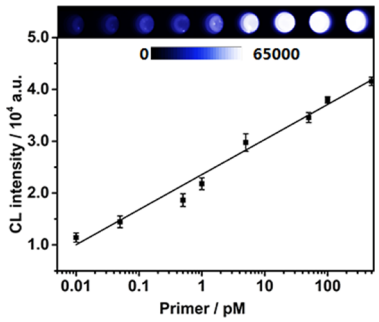

Figure 4. CL signals at 0.01, 0.05, 0.5, 1, 5, 50, 100, and 500 pM primer and the plot of the CL signal vs the logarithm of primer concentration.

Analytical Performance of CL Assay to the SARS-CoV-2 Protein. The concentrations of Ab-1 and Ab-2 had an impact on the CL signal and the detection range. At different concentrations of Ab-1 and Ab-2, the CL intensity increased and then decreased with the increasing concentration of the SARS-CoV-2 protein (Figure 5A). The signal decrease was caused by the Hook effect.[36] Considering the widest detection range and the appropriate sensitivity, 10 ng/mL DNA–antibody conjugates were chosen.

Under the optimal conditions, the CL intensity increased with the increasing concentration of the SARS-CoV-2 protein from 0.02 to 100 pg/mL (Figure 5B), and the plot of the CL signal versus the logarithm of the SARS-CoV-2 protein concentration showed good linearity with a linear equation of $I = 8.3 \log c + 29.8$. The limit of detection was estimated to be 6.46 fg/mL ($3S_b/m$, where S_b is the standard deviation of the blank signal ($n = 20$) and m is the slope of the calibration curve). This remarkable sensitivity of the proposed CL assay was attributed to the large amount of G4 sequences produced in RCA. The selectivity of this CL assay for the SARS-CoV-2 protein was confirmed by comparing the CL signals in the presence of different proteins, including PCSK9, PSA, AFP, CEA, and BSA. As expected, these proteins did not show a

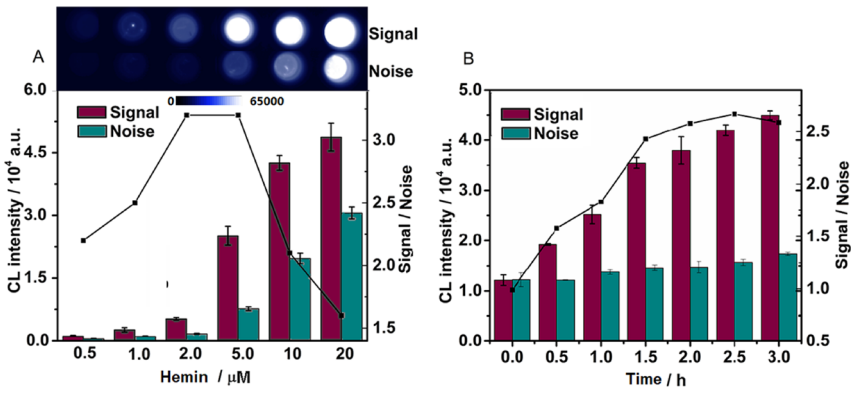

Figure 3. CL signals and signal-to-noise ratios at different hemin concentrations (A) and reaction times (B).

https://doi.org/10.1021/acs.analchem.1c02229
Anal. Chem. 2021, 93, 9933−9938

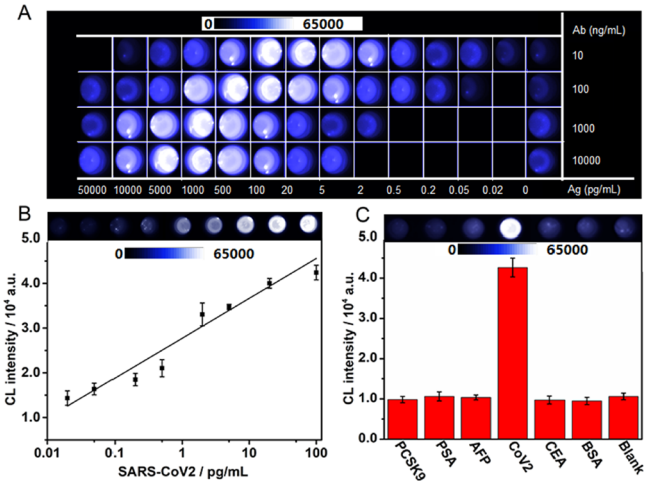

Figure 5. (A) CL imaging at different SARS-CoV-2 concentrations detected with 10, 100, 1000, and 10,000 ng/mL Ab-1 and Ab-2. (B) CL signals at 0.02, 0.05, 0.2, 0.5, 2, 5, 20, and 100 pg/mL SARS-CoV-2 and the corresponding calibration curve. (C) CL responses to 20 pg/mL PCSK9, PSA, AFP, SARS-CoV-2, CEA, BSA, and PBS.

significant signal in comparison with the blank, while the target showed an extremely increased signal (Figure 5C), which demonstrated that these proteins did not interfere with the detection and the proposed method had excellent specificity.

Real Sample Analysis. Recovery experiments were applied to examine the accuracy of SARS-CoV-2 protein analysis by mixing various concentrations of the SARS-CoV-2 protein with human serum samples. As shown in Table 1, the recovery rate ranged from 80.0 to 91.4%, which indicated the acceptable reliability of this method.

Table 1. Detection Results of the SARS-CoV-2 Protein Added in Serum Samples

number	added (pg/mL)	measured (pg/mL)	recovery (%)
1	0.02	0.016	80.0
2	0.5	0.436	87.2
3	5	4.57	91.4
4	100	83.2	83.2

The sensitivity of the CL imaging method was further evaluated with the SARS-CoV-2 vaccine. Different concentrations of the SARS-CoV-2 vaccine were detected using both commercial GICA and CL assay. As shown in Figure 6A, in the absence of the SARS-CoV-2 vaccine, the GICA assay displayed only a red band at the top, which demonstrated that the test result was negative. After 290 or 580 pg/mL SARS-CoV-2 vaccine was introduced into the detection solution, no new band occurred on the test paper. The existence of 5.8 ng/mL SARS-CoV-2 vaccine resulted in a slight red band at the bottom of the test paper, which got darker at a concentration of 58 ng/mL. However, the suggested method showed the CL signal at the SARS-CoV-2 vaccine concentrations lower than 0.58 pg/mL (Figure 6B), indicating obviously higher sensitivity in comparison with the GICA assay.

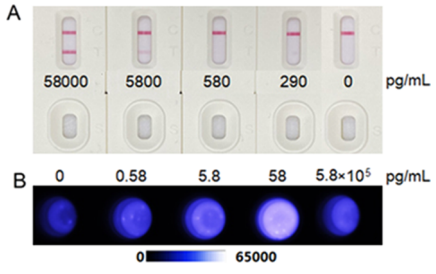

Figure 6. (A) GICA test of the SARS-CoV-2 vaccine at 58,000, 5800, 580, 290, and 0 pg/mL. (B) CL detection of the SARS-CoV-2 vaccine with the proposed method at 0, 0.58, 5.8, 58, and 5.8 × 10^5 pg/mL.

CONCLUSIONS

A highly sensitive CL imaging system for quantitative detection of the SARS-CoV-2 protein has been proposed by target-induced formation of a G4/hemin DNAzyme. The homogeneous CL imaging procedure can be conveniently performed by mixing the sample with a pair of DNA−antibody conjugates, a circular DNA, a block/primer complex, and a RCA reaction solution to simultaneously trigger proximity hybridization, strand displacement reaction, and RCA, which produces a large amount of G4 duplicate sequences for forming abundant horseradish peroxidase-like DNAzyme units in the presence of hemin. The amplified CL imaging method for the SARS-CoV-2 protein shows a wide concentration range along with a fg/mL-level detection limit and good selectivity. Owing to the advantages of CL analysis and intrinsic high throughput of the imaging technique, the proposed CL assay possesses the potential applicability in early screening and prompt diagnosis of the SARS-CoV-2 disease.

ASSOCIATED CONTENT

Supporting Information

The Supporting Information is available free of charge at https://pubs.acs.org/doi/10.1021/acs.analchem.1c02229.

Oligonucleotide sequences (PDF)

AUTHOR INFORMATION

Corresponding Authors

Qiang Wu − *School of Tropical Medicine and Laboratory Medicine, Key Laboratory of Emergency and Trauma of Ministry of Education, Hainan Medical University, Haikou 571199, China*; Phone: +86-898-66984599; Email: wuqiang001001@aliyun.com

Huangxian Ju − *State Key Laboratory of Analytical Chemistry for Life Science, School of Chemistry and Chemical Engineering, Nanjing University, Nanjing 210023, China*; orcid.org/0000-0002-6741-5302; Phone: +86-25-89683593; Email: hxju@nju.edu.cn

Authors

Rui Zhang − *School of Tropical Medicine and Laboratory Medicine, Key Laboratory of Emergency and Trauma of Ministry of Education, Hainan Medical University, Haikou 571199, China*

Jie Wu − *State Key Laboratory of Analytical Chemistry for Life Science, School of Chemistry and Chemical Engineering, Nanjing University, Nanjing 210023, China*; orcid.org/0000-0003-1379-122X

Hang Ao − *State Key Laboratory of Analytical Chemistry for Life Science, School of Chemistry and Chemical Engineering, Nanjing University, Nanjing 210023, China*

Jinling Fu − *School of Tropical Medicine and Laboratory Medicine, Key Laboratory of Emergency and Trauma of*

https://doi.org/10.1021/acs.analchem.1c02229
Anal. Chem. 2021, 93, 9933−9938

Ministry of Education, Hainan Medical University, Haikou 571199, China

Bin Qiao − *School of Tropical Medicine and Laboratory Medicine, Key Laboratory of Emergency and Trauma of Ministry of Education, Hainan Medical University, Haikou 571199, China*

Complete contact information is available at: https://pubs.acs.org/10.1021/acs.analchem.1c02229

Notes

The authors declare no competing financial interest.

■ ACKNOWLEDGMENTS

We acknowledge financial support from the National Natural Science Foundation of China (nos. 81860373 and 82060386), the Finance Science and Technology Project of Hainan Province (no. 2019RC221), the CAMS Innovation Fund for Medical Sciences (no. 2019-I2M-5-023), and the Science and Technology Project of 2019-nCoV of the Hainan Medical University (no. XGZX2020008).

■ REFERENCES

(1) Mariën, J.; Ceulemans, A.; Michiels, J.; Heyndrickx, L.; Kerkhof, K.; Foque, N.; Widdowson, M. A.; Mortgat, L.; Duysburgh, E.; Desombere, I.; Jansens, H.; Van Esbroeck, M.; Ariën, K. K. *J. Virol. Methods* **2021**, *288*, 114025−114031.
(2) Chaimayo, C.; Kaewnaphan, B.; Tanlieng, N.; Athipanyasilp, N.; Sirijatuphat, R.; Chayakulkeeree, M.; Angkasekwinai, N.; Sutthent, R.; Puangpunngam, N.; Tharmviboonsri, T.; Pongraweewan, O.; Chuthapisith, S.; Sirivatanauksorn, Y.; Kantakamalakul, W.; Horthongkham, N. *Virol. J.* **2020**, *17*, 177−185.
(3) Perlman, S.; Netland, J. *Nat. Rev. Microbiol.* **2009**, *7*, 439−450.
(4) Elmokadem, A. H.; Batouty, N. M.; Bayoumi, D.; Gadelhak, B. N.; Abdel-Wahab, R. M.; Zaky, M.; Abo-Hedibah, S. A.; Ehab, A.; El-Morsy, A. *Insights Imaging* **2021**, *12*, 12−30.
(5) Lenicek Krleza, J.; Zrinski Topic, R.; Stevanovic, V.; Lukic-Grlic, A.; Tabain, I.; Misak, Z.; Roic, G.; Kaic, B.; Mayer, D.; Hruskar, Z.; Barbic, L.; Vilibic-Cavlek, T. *Biochem. Med.* **2021**, *31*, 020706−020718.
(6) Liu, P. P.; Zong, Y.; Jiang, S. P.; Jiao, Y. J.; Yu, X. J. *ACS Omega* **2021**, *6*, 9667−9671.
(7) Villalta, D.; Martelli, P.; Moratto, A.; Salgarolo, V.; Ligato, E.; Conte, M.; Giacomello, R.; Pellis, T.; De Rosa, R.; Venturini, S.; Crapis, M. *Pract. Lab. Med.* **2021**, *25*, e00227−e00227.
(8) Hatmal, M. M.; Alshaer, W.; Al-Hatamleh, M. A. I.; Hatmal, M.; Smadi, O.; Taha, M. O.; Oweida, A. J.; Boer, J. C.; Mohamud, R.; Plebanski, M. *Cells* **2020**, *9*, 2638−2675.
(9) Rebai, A.; Souissi, A.; Abid, N.; Masmoudi, S. *EuroMediterr. J. Environ. Integr.* **2021**, *6*, 40−45.
(10) Zhang, Z.; Wang, X.; Wei, X.; Zheng, S. W.; Lenhart, B. J.; Xu, P.; Li, J.; Pan, J.; Albrecht, H.; Liu, C. *Biosens. Bioelectron.* **2021**, *181*, 113134.
(11) Tang, Y.; Zhai, Y. F.; Xiang, J. J.; Wang, H.; Liu, B.; Guo, C. W. *Environ. Pollut.* **2010**, *158*, 2074−2077.
(12) Shen, B.; Zheng, Y.; Zhang, X.; Zhang, W. T.; Wang, D. L.; Jin, J.; Lin, R.; Zhang, Y.; Zhu, G. J.; Zhu, H. G.; Li, J.; Xu, J. Q.; Ding, X. H.; Chen, S. Y.; Lu, R. Y.; He, Z. B.; Zhao, H. H.; Ying, L. J.; Zhang, C.; Lv, D.; Chen, B.; Chen, J.; Zhu, J.; Hu, B.; Hong, C.; Xu, X.; Chen, J.; Liu, C.; Zhou, K.; Li, J.; Zhao, G.; Shen, W.; Chen, C.; Shao, C.; Shen, X.; Song, J.; Wang, Z.; Meng, Y.; Wang, C.; Han, J.; Chen, A.; Lu, D.; Qian, B.; Chen, H.; Gao, H. *Am. J. Transl. Res.* **2020**, *12*, 1348−1354.
(13) Singh, A.; Seo, Y. H.; Lim, C. K.; Koh, J.; Jang, W. D.; Kwon, I. C.; Kim, S. *ACS Nano* **2015**, *9*, 9906−9911.
(14) Liao, B. Y.; Chang, C. J.; Wang, C. F.; Lu, C. H.; Chen, J. K. *Sens. Actuators B-Chem.* **2021**, *336*, 129710−129722.
(15) Cao, M.; Liu, Y.; Lu, C.; Guo, M.; Li, L.; Yu, C.; Wei, J. F. *Anal. Methods* **2021**, *13*, 2478−2484.
(16) Saito, K.; Chang, Y. F.; Horikawa, K.; Hatsugai, N.; Higuchi, Y.; Hashida, M.; Yoshida, Y.; Matsuda, T.; Arai, Y.; Nagai, T. *Nat. Commun.* **2012**, *3*, 1262−1271.
(17) Li, D.; Li, J. *J. Clin. Microbiol.* **2021**, *59*, 02160−02172.
(18) Lee, J. J.; White, A. G.; Rice, D. R.; Smith, B. D. *Chem. Commun.* **2013**, *49*, 3016−3018.
(19) Gübitz, G.; Schmid, M. G.; Silviaeh, H.; Aboul-Enein, H. Y. *Anal. Chem.* **2001**, *31*, 141−148.
(20) Zong, C.; Wu, J.; Wang, C.; Ju, H.; Yan, F. *Anal. Chem.* **2012**, *84*, 2410−2415.
(21) Zong, C.; Wu, J.; Xu, J.; Ju, H.; Yan, F. *Biosens. Bioelectron.* **2013**, *43*, 372−378.
(22) Xu, J.; Wu, J.; Zong, C.; Ju, H.; Yan, F. *Anal. Chem.* **2013**, *85*, 3374−3379.
(23) Zong, C.; Wu, J.; Liu, M.; Yang, L.; Liu, L.; Yan, F.; Ju, H. *Anal. Chem.* **2014**, *86*, 5573−5578.
(24) Liu, M.; Wu, J.; Yang, K.; Zong, C.; Lei, J.; Ju, H. *Talanta* **2016**, *154*, 455−460.
(25) Zong, C.; Wu, J.; Liu, M.; Yang, L.; Yan, F.; Ju, H. *Anal. Chem.* **2014**, *86*, 9939−9944.
(26) Dean, F. B.; Nelson, J. R.; Giesler, T. L.; Lasken, R. S. *Genome Res.* **2001**, *11*, 1095−1099.
(27) Liao, X.; Zhang, C.; Shi, Z.; Shi, H.; Qian, Y.; Gao, F. *J. Electroanal. Chem.* **2020**, *878*, 114604.
(28) Liu, L. Q.; Yin, F.; Lu, Y.; Yan, X. L.; Wu, C. C.; Li, X.; Li, C. *Nanomedicine* **2021**, *32*, 102339−102346.
(29) Xie, Y.; Niu, F.; Yu, A.; Lai, G. *Anal. Chem.* **2020**, *92*, 593−598.
(30) Wang, C.; Wu, J.; Zong, C.; Ju, H.; Yan, F. *Analyst* **2011**, *136*, 4295−4300.
(31) Xiao, Y.; Pavlov, V.; Gill, R.; Bourenko, T.; Willner, I. *ChemBioChem* **2004**, *5*, 374−379.
(32) Yang, H.; Zhou, Y.; Liu, J. *TrAC Trends Anal. Chem.* **2020**, *132*, 116060−116094.
(33) Yang, K.; Huo, M.; Guo, Y.; Yang, Y.; Wu, J.; Ding, L.; Ju, H. *Analyst* **2017**, *142*, 3740−3746.
(34) Ren, K.; Wu, J.; Ju, H.; Yan, F. *Anal. Chem.* **2015**, *87*, 1694−1700.
(35) Mergny, J. L.; Li, J.; Lacroix, L.; Amrane, S.; Chaires, J. B. *Nucleic Acids Res.* **2005**, *33*, e138−e145.
(36) Chen, W.; Shan, S.; Peng, J.; Liu, D.; Xia, J.; Shao, B.; Lai, W. *Sensor. Actuat. B-Chem.* **2020**, *321*, 128465−128473.